# An NMR Imaging Study of Methanol Desorption from Partially Swollen PMMA Rods

**L. A. Weisenberger and J. L. Koenig***

*Department of Macromolecular Science, Case Western Reserve University, Cleveland, Ohio 44106.* *Received August 4, 1989; Revised Manuscript Received December 5, 1989*

ABSTRACT: This NMR imaging investigation shows several previously undetected features of methanol desorption from PMMA. The desorption is characterized by decreases in signal intensities in the images and by changes in calculated images representing time constants for exponential intensity decays from several magnitude images. Three regions in the partially swollen polymer show widely varying desorption characteristics, the surface region, the region surrounding the glassy core, and the bulk region between them. The apparent controlling feature of the desorption process at any point is the polymer segmental motions restricting the solvent mobility.

## Introduction

The diffusion and desorption of small molecules are important to the material properties of polymers from processing and production to end use and shelf-life. Although much interest surrounds the migration of plasticizers and other small molecules in polymers, little information is available on the physical distribution of these molecules within the polymer or on the mechanism by which desorption occurs. Much of the literature work employs gravimetric techniques to determine absorption and desorption rates. Differences in these rates or deviations from ideal behavior are utilized to imply polymer and diluent interactions and structures. Some techniques such as electron spin resonance (ESR) provide more direct information but utilize doping procedures to provide the signal rather than directly examining the diluent.[1] Even optical microscopy,[2] which provides visual information of the diluent distribution, requires doping to enhance the contrast between the polymer and the solvent. Furthermore, most techniques require stopping the diffusion process and destroying the sample.

NMR imaging is a new technique utilized in polymer science. It is primarily sensitive to protons on mobile solvent molecules and as such is particularly well-suited for studying diffusion processes of small molecules. It provides a visual presentation of the spatial distribution of diluent in the polymer by acquiring signal directly from the protons of the solvent without interrupting the diffusion process or destroying the sample. Hence, the diffusion process may be studied as long as desired on a single sample eliminating many of the systematic errors associated with other techniques.

Several studies have employed NMR imaging as a tool to examine solvents in polymers[3-5] and several groups have demonstrated the utility of NMR imaging for studying diffusion in polymers.[6-8] In particular, studies from this lab show the ability of NMR imaging to follow Case II transport of organic solvents in PMMA[9-11] and the versatility of NMR imaging for studying self-diffusion and molecular motions[12] associated with Case II diffusion processes. Further information on the details and applications of NMR imaging is available in several reviews.[13-21]

Desorption is one diffusion process that has had little attention primarily due to the lack of adequate analytical techniques. NMR imaging provides the spatial distribution of solvent in the polymer as well as the spatial distribution of the rate of desorption as described in this paper.

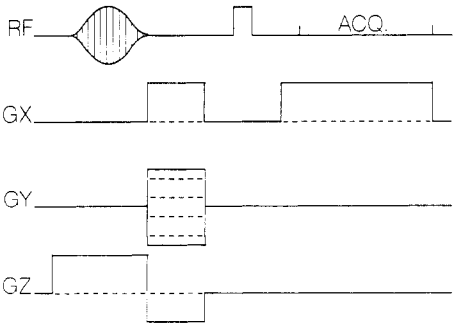


**Figure 1.** The timing diagram for the spin-echo imaging pulse sequence.

## Experimental Section

The imaging system is based on the Bruker MSL 300 spectrometer with mini- and microimaging. The microimaging probe is used for this investigation. The gradients are generated by using gradient coils inside of the probe. Gradient amplification is achieved with NAD amplifiers and pre- and post-emphasis are used in all cases. Gradient strength for the read direction is 8.4 G $cm^{-1}$ producing a resolution of 68 $\mu m$ $pixel^{-1}$. Gaussian-shaped pulses are generated by using a selective excitation unit and are 1 ms in duration. These shaped pulses along with a $z$-gradient produce a slice thickness of 2 mm. The nonselective 180° pulses are 81 $\mu s$. The echo time is 5.08 ms. The repetition time used is 3 s.

The imaging pulse sequence is based on the spin-echo pulse sequences of Carr and Purcell[22] and Meiboom and Gill.[23] Figure 1 is the spin-echo imaging pulse sequence. The 90° pulse tips the magnetization into the $x'$-$y'$ plane where it begins dephasing. The 180° pulse is applied after a time $\tau$, forcing the magnetization to refocus at $2\tau$ (also known as the echo time, TE) after the 90° pulse. The acquisition is centered around $2\tau$. Frequency-encoding gradients, GX, cause the spins to precess at different frequencies depending on their position in the magnetic field. Phase-encoding gradients, GY, are orthogonal to GX and cause the spins to dephase at different rates providing the second dimension of a two-dimensional image. The slice selection gradient, GZ, and the Gaussian-shaped 90° pulse determine the position and thickness of the region of interest. The data are Fourier transformed in two dimensions to produce the image. More details on NMR imaging are available in numerous reviews.[13-21]

The samples are lightly cross-linked PMMA rods, 12.7 mm in diameter from Commercial Plastics and Supplies Corp., Cleveland, OH. The methanol is deuterated at the hydroxy position (99.5%) and is used as received from Aldrich Chemical. Each sample is submersed in the methanol at 30 °C until the desired swelling is achieved. The methanol volume fraction is 0.26 from previous studies.[9-11] The rod is then place in fully deuterated cyclohexane (Aldrich Chemical, 99.5% substituted) at 30 °C.

0024-9297/90/2223-2454$02.50/0 

The first image acquisition began 6 min after initial submersion. The remaining images began at 1-h increments over 104 h. Images are transferred from the Aspect 3000 computer of the imaging system to a MicroVax II via Ethernet communications. They are then processed by using software written in Fortran 77 by J. Liu of this group. $T_d$ images are generated from several images using T2EXP. This program is a nonlinear least-squares fits on a pixel-by-pixel basis to eq 1. The result

$$M = M_0 \exp(-T_{exp}/T_d) \quad (1)$$

is a calculated image with its intensity based on the parameter $T_d$ with higher intensities indicating larger $T_d$s. $T_d$ with higher intensities indicating larger $T_d$s. $T_d$ is the inverse of the rate of intensity loss with respect to exposure time to cyclohexane, $T_{exp}$. In the absence of relaxation effects, (in this case $T_2$ effects since the images were acquired with a repetition time of 5 $T_1$), $T_d$ is the inverse of the rate of net solvent loss for a given pixel. It does not represent the solvent flux or total mass through the pixel.

An image was acquired of a partially swollen rod in perdeuterated methanol. The image showed no signal due to the PMMA in the swollen region under the same conditions of these experiments.

## Results

A part of the series of images, acquired initially and every 10 h after submersion in cyclohexane, is shown in Figure 2. This series represents the 104 images collected. In these images, red represents the highest intensity and dark blue is the lowest with the green, yellow, and orange representing the intermediate intensity levels in increasing order. The signal intensities decrease over time as seen in the images in Figure 2. These decreases are seen more quantitatively in Figure 3 which is a series of profiles from each of the images in Figure 2. The decrease in the maximum intensity from the first image to the last is 50% over the 100-h interval. The diameter of the rod decreases by 816 ± 68 μm over the 100 h as measured from the images. The diameter measure with a micrometer shows a 150 ± 68 μm decrease. The diameter of the glassy core decreases by 272 ± 68 μm by 40-h exposure time and maintains that diameter for the remainder of the exposure.

In order to further quantify the desorption of methanol from the PMMA rod, several images are used in the fitting procedure described in the Experimental Section. A $T_d$ image calculated from 20 images taken at 5-h increments over 100 h (1, 6, 11, ..., 101 h) is shown in Figure 4. In this image red represents the largest $T_d$ and dark blue represents the smallest $T_d$ corresponding to the slowest and fastest intensity decreases, respectively. This image shows the faster intensity decreases are near the surface of the rod and the slower are near the glassy PMMA core. The $T_d$ at the surface is 58 h and the $T_d$ at the glassy core is 450 h from this image.

An alternative procedure is to fit consecutive images to eq 1 rather than every fifth image as described in the previous paragraph. A series of $T_d$ images calculated from 20 consecutive images starting at different times (the first image includes 20 spin-echo images from 1 to 20 h, the second includes images from 21 to 40 h, etc.) are shown in Figure 5. Figure 5A is similar to Figure 4 in that the larger $T_d$s are at the glassy core, and the smaller are closer to the surface. However considerable differences are evident between the two images. Figure 5A shows $T_d$ near the glassy core, that is so large that it cannot be effectively measured on a 100-h time scale. This large $T_d$ occurs 1.71 mm out from the glassy core where the $T_d$ drops rapidly. The $T_d$ drops to a minimum of 62 h at 3.49 mm from the glassy core and rises again to 109 h at the surface of the rod.

Figure 5B includes images from 21 h through 40 h. Like Figure 5A, Figure 5B shows long $T_d$s near the glassy core and smaller $T_d$s away from the core. Several changes have occurred from the first calculated image. The $T_d$s near the glassy core are 600 h, a large decrease from the first 20 h. The $T_d$ at 3.49 mm where the minimum occurred in the previous image is now 120 h. At the surface of the rod the $T_d$ is now 66 h.

Figure 5C is calculated with images from 41 to 60 h. Again the higher $T_d$ values are near the glassy core, but the values are reduced to 400 h. The $T_d$ values decrease from the core out to the surface. Figure 5D is calculated with images from 61 to 80 h and shows a $T_d$ of 200 h near the glassy core and a value of 150 h in the remaining swollen regions. Figure 5E is calculated with images from 81 to 100 h and has a uniform $T_d$ of 150 h.

## Discussion

One of the many unique characteristics of polymers is the range of diffusion processes they exhibit. Case II diffusion occurs when small organic molecules diffuse into an amorphous polymer that is below its $T_g$. It is characterized by (1) a sharp concentration gradient occurs at the interface between the swollen and nonswollen regions of the sample, (2) the solvent concentration in the swollen regions is constant, and (3) the sharp front moves into the nonswollen polymer at a constant speed.[24,25] The diffusion of methanol into PMMA exhibits Case II diffusion and is well-characterized by several techniques[24,25] including NMR imaging.[9-11] This work represents an effort to look at the opposite effect, the desorption of solvent from the polymer. The PMMA/methanol system was selected so as to utilize the unique characteristics of Case II diffusion. Since the solvent concentration is constant in the swollen regions, for a pure spin-density image, the intensity of an NMR image is constant wherever solvent is present. The initial constant concentration permits easier analysis of initial relaxation effects as discussed in previous papers.[11,12]

Solvent desorption from polymers has been studied by using not only primarily gravimetric techniques but also techniques such as ESR[1] and birefringence measurements.[2] Desorption measurements above the glass transition temperature $T_g$ of the unswollen polymer are expected to follow Fickian characteristics. Likewise, polymers swollen so that $T_g$ is below the experimental temperature initially exhibit Fickian desorption. The solvent is thought to desorb rapidly from the surface of the polymer, raising the $T_g$ of the surface layer. After the surface $T_g$ is above the experimental temperature, the desorption process slows and the process is controlled by the diffusion through the glassy surface layer.[2,28] This work extends these ideas from macroscopic desorption rates to show the distribution of solvent and desorption rates within a partially swollen sample.

As described in a previous paper,[11] the imaging experiment time must be compared to the desorption process to determine to what extent artifacts are generated by the solvent movement. The first aspect is the relationship of the delay time, spin–lattice ($T_1$) relaxation, and the desorption rate. The longest $T_1$ observed in a PMMA sample swollen with methanol[12] is 0.6 s which requires a relaxation time of 3 s as used here. Therefore, little $T_1$ saturation is observed. As the polymer becomes less swollen, the $T_1$s decrease so that 3 s is sufficient for the entire set of images.

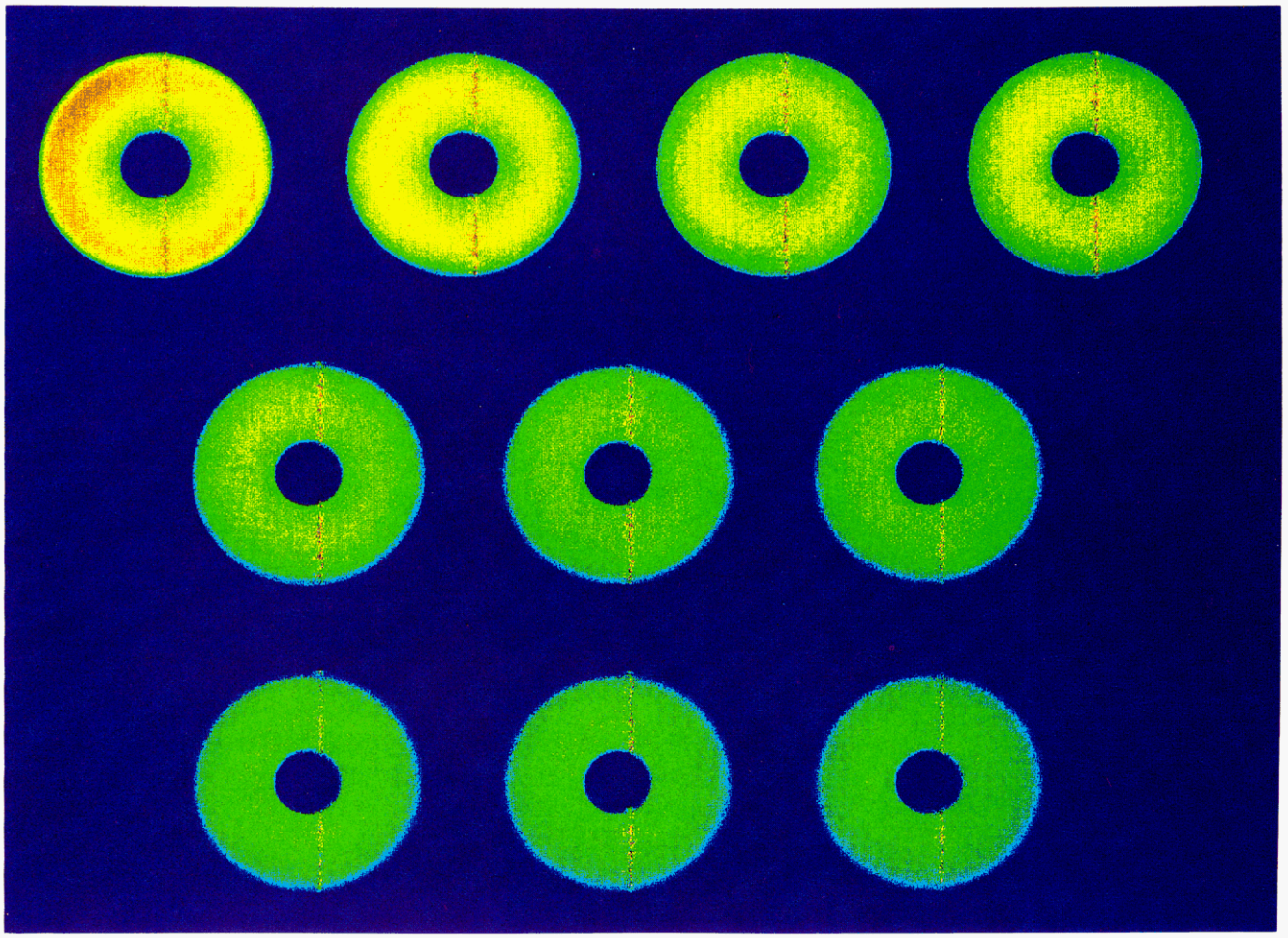

**Figure 2.** A representative set of spin-echo images acquired after different exposure times to cyclohexane (reading from upper left to lower right): (A) 6 min, (B) 10, (C) 20, (D) 30, (E) 40, (F) 50, (G) 60, (H) 70, (I) 80, and (J) 90 h.

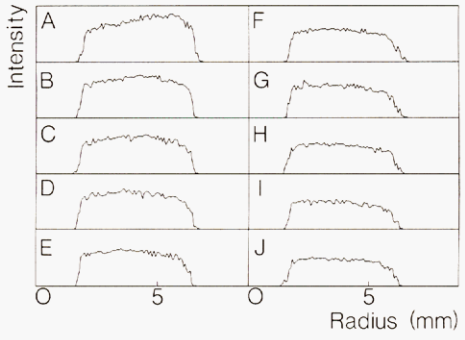


**Figure 3.** Intensity profiles from the images in Figure 2 (reading from upper left to lower right): (A) 6 min, (B) 10, (C) 20, (D) 30, (E) 40, (F) 50, (G) 60, (H) 70, (I) 80, and (J) 90 h.

Since a 3-s delay time takes 51 min with 256 phase-encoding steps and phase cycling, significant movement of the solvent is possible. Changes in intensity due to moving solvent boundries during a NMR imaging experiment impart artifacts on the overall image due to the phase-encoding process.[11] Since desorption does not follow Case II characteristics, the artifacts, if any, it imposes on the images are difficult to describe. However, on the basis of the previous simulations and results for Case II diffusion,[11] the largest artifacts are caused by large intensity changes over the imaging time in any given region of the image. The intensity decrease from the first to the second image is less than 10%, and the decreases between later images are even smaller. Therefore, artifacts due to solvent movement associated with desorption are small. Furthermore, these types of artifacts occur as intensity modulations most pronounced in the phase-encoding direction. No such modulations are observed in these images, and motion artifacts are considered negligible in this study.

Previous studies[11,12] with spin-echo images demonstrate unexpected changes in intensities due to decreased $T_2$s caused by restricted polymer and solvent mobility nearing the glassy core. The same $T_2$ contrast is apparent in these magnitude images. Figure 2A shows a decrease in intensity from the surface of the polymer to the glassy core that is associated with $T_2$ attenuation. A true spin-density image exhibits a flat intensity profile since the methanol concentration is constant from the surface to the glassy core. In general, the methanol $T_2$s decrease with decreasing solvent concentration due to the decreasing mobility of the solvent and the polymer chains. Since the contributions from the $T_2$ attenuation and the methanol desorption to the decreased signal intensities are unknown and complex, the contributions are assumed equal. Therefore, the $T_d$s reported here are smaller than those expected for pure desorption. The $T_d$s are comparable throughout the sample since the decreases in $T_2$s are likely to follow the decrease in solvent concentration closely.

At this point, it is worth mentioning that the $T_g(0)$ of the PMMA/methanol system is estimated to be 296 K according to eq 2 given by Fox[26] where $T_{gx}$ are the $T_g$s

$$\frac{1}{T_{gr}} = \frac{\omega_p}{T_{gp}} + \frac{\omega_s}{T_{gs}} \qquad (2)$$

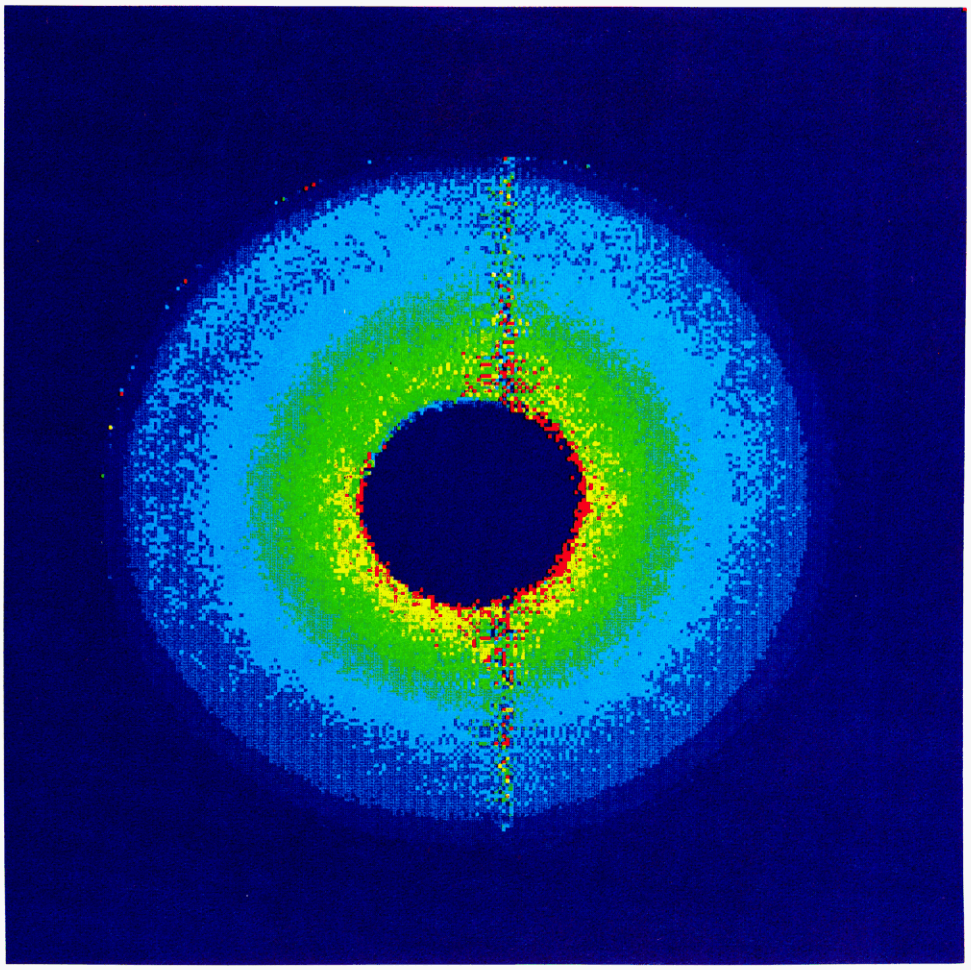

**Figure 4.** A $T_d$ image calculated from 20 images like those in Figure 2 at 5-h increments over a 100-h interval.

of the rubber (x = r), polymer (x = p), and solvent (x = s) and $\omega_x$ are the weight fractions of the polymer and the solvent. Since the system $T_g$ is only 7° below the experimental temperature, little desorption is required to raise the $T_g$ above it. The volume fraction where the system $T_g$ is equal to the experimental temperature is 0.23 which is only a 12% decrease from the volume fraction measured previously.[9-11]

The methanol concentration is clearly decreasing with time as indicated by the signal intensity losses in the images of Figure 2. $T_d$ images provide a visual representation of the solvent desorption rate. Recall that $T_d$s are considered proportional to the inverse of the desorption rates so that large $T_d$s represent slow desorption rates. Figure 3 is a $T_d$ image generated from images over the 100-h interval of the desorption experiment. It shows that the desorption rates are slow near the glassy core and fast near the polymer surface. This agrees with Fickian characteristics which indicate that imbibed solvent near the surface desorbs quickly and the desorption rates decrease toward the sample core. However, Figure 3 shows no indication of a glassy skin developing on the polymer surface as discussed by other researchers.[2,27,28] The skin should be represented by larger $T_d$s (brighter areas) since it reportedly develops glassy characteristics and slower rates early in the desorption process.

Unfortunately when generating these $T_d$ images, the shapes of the calculated curves for each pixel and how well they fit the data are difficult to visualize. Furthermore, if visualization of the fitted curves is possible, the number of curves per image is excessive to analyze on a pixel-by-pixel basis. An alternative is to fit images taken during different time intervals. If the desorption rates occur as single exponential decays, then the $T_d$ images from different time intervals are similar. If the desorption rates vary in time, then the images are different. Since the form of the fitting equation is not obvious, other forms may provide better fits. However, only exponential decays were used in this work.

The images collected over 100 h are divided into 20-h time intervals to generate the five $T_d$ images in Figure 5. Because of the detailed structures obtained with these calculated images this discussion is limited to the three stages of desorption that are most apparent from these images and to three regions in each image, the surface region, the core region around the unswollen polymer glass, and the bulk region between the others.

The first stage (Figure 5A) is a very small $T_d$ from the bulk with a larger $T_d$ at the polymer surface. The first stage also has a $T_d$ around the glassy core that is several orders of magnitude above the bulk. In the second stage (Figure 5B,C), the $T_d$ from the bulk is uniform everywhere except around the glassy core where the $T_d$ is much smaller than in the first stage but still larger than the bulk. In the third stage (Figure 5D,E), the $T_d$s are nearly constant throughout the entire swollen region. When the images are divided into 10-h time intervals, few differences are observed from those in Figure 5 indicating that the 20-h intervals are sufficient to adequately describe the desorption process.

The first stage is the most interesting because of the wide range of $T_d$s. Another unique feature of the first stage is that the surface appears to have larger $T_d$s than the bulk region. Desorption should initially occur most

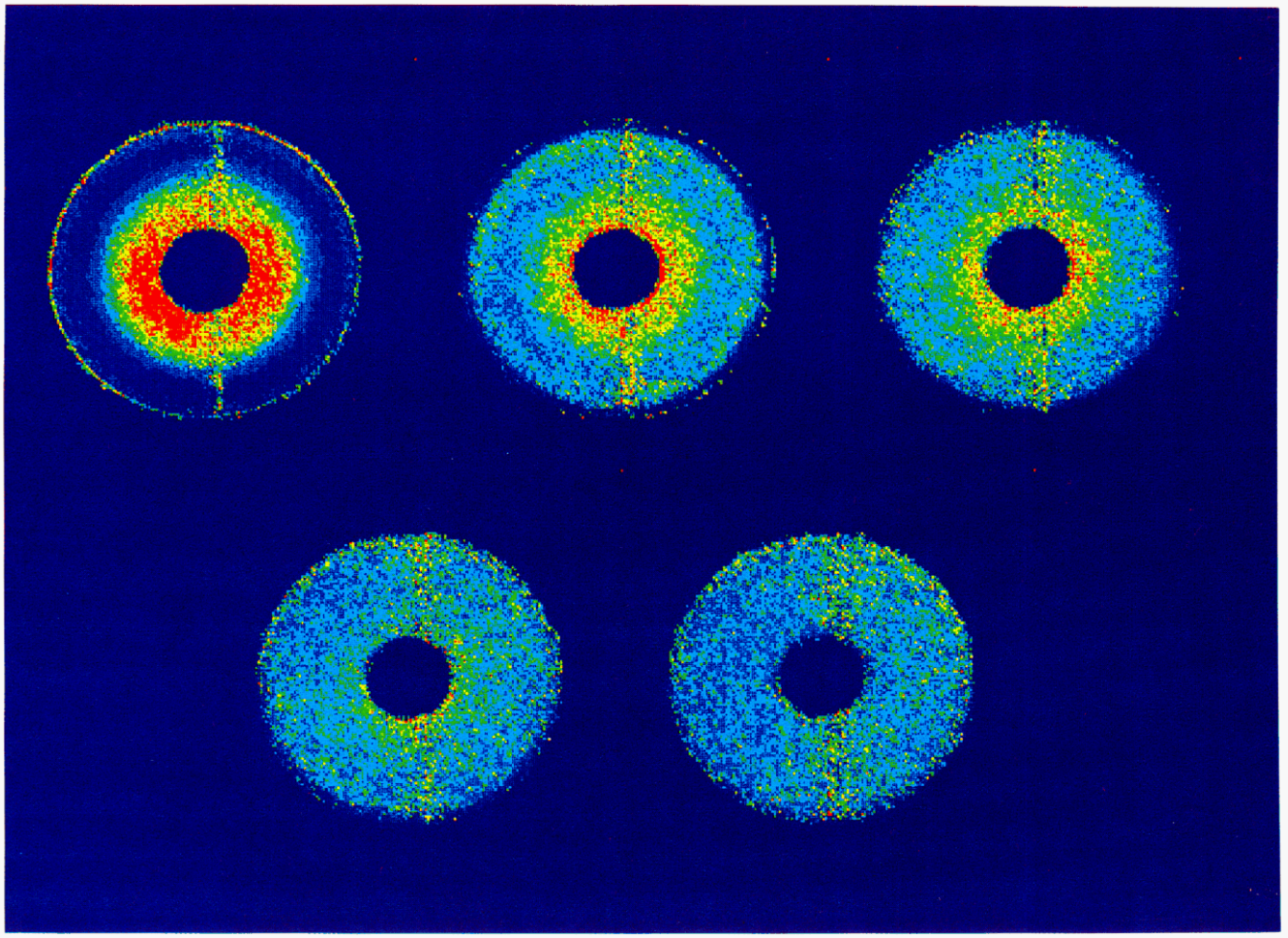

**Figure 5.** $T_d$ images calculated from 20 images like those in Figure 2 at 1-h increments over 20-h intervals (reading from upper left to lower right): (A) 1–20, (B) 21–40, (C) 41–60, (D) 61–80, and (E) 81–100 h.

rapidly at the surface which would be indicated by a deep shade of blue. However, in the $T_d$ image methanol appears to desorb at slower rates at the surface than in the bulk (Figure 5A). While a contradiction seems to exist between these data and previous work, the difference is most likely to be the result of the imaging experiment requiring too much time relative to the desorption rate at the surface. In the magnitude images (Figure 2A–C) associated with this time interval, a deep shade of blue ring is at the rod surface indicating a low methanol concentration. The low intensity indicates that the surface concentration drops so rapidly that the imaging experiment does not acquire the surface signal quickly enough to accurately reflect the initial surface concentration. The rapid surface concentration decrease is further confirmed by the difference between the outer diameter measured from images and measured with a micrometer. The micrometer reading is larger than the diameter from the image, indicating that little solvent signal is coming from the surface. In order to capture the initial surface concentration and its rapid decrease, several images would have to be collected in the first few minutes after initial exposure to cyclohexane. The rapid acquisition required is not possible with current NMR instrumentation, so the initial images and the $T_d$ image indicate the desorption rates from the surface after the surface has become glassy are slower than the initial or the bulk rates.

The $T_d$s in the bulk region are smaller than those at the surface. Again this seems unreasonable, since the glassy surface should be limiting the desorption rate. Two possible sources contribute to this anomaly. One factor is although the surface is limiting the bulk desorption rate, the $T_d$ represents the decrease in solvent concentration for that region only and not the flux through the region. The solvent from the bulk polymer must desorb through the glassy surface. The methanol desorbing from the bulk maintains the concentration in the surface so that the desorption rates at the surface region appear to be slower since the desorption out of the surface region is partially compensated by the desorption from the bulk region. So the net transport from the region is much smaller than the total methanol transported through the region. The desorption rate in the bulk is faster because it is still rubbery. Another factor is the diffusion into the glassy core which continues even as methanol desorbs from the surface and the bulk. The sharp methanol front advances 136 ± 68 $\mu$m during the first 40 h that the system is monitored. The continued diffusion into the glassy core draws the necessary methanol from the bulk supply giving a $T_d$ that is smaller than surface desorption alone.

Another interesting feature of the $T_d$ image for the first 20 h is the region near the glassy core. The core region is clearly defined by the dramatic intensity increase over a short distance from the bulk. The $T_d$ in this region is so large that it cannot be accurately measured on a 100-h time scale. This indicates that no solvent is lost in this region during the first 20 h.

If the desorption is purely osmotic pressure driven and exhibits Fickian characteristics, the concentration profiles and the $T_d$s increase toward the glassy core. The desorption rate profiles decrease toward the glassy core.

The simplest explanation of the extremely large $T_d$s in the core region is that the desorption front has not progressed far enough into the sample for any desorption to occur in that region. Another factor is that the sharp methanol front continues to advance by 136 $\mu$m, thereby contributing to the high $T_d$s by drawing more solvent into the region to continue diffusion into the glassy core, although the front speed is considerably slower than previously reported[9-11] due to the decreasing methanol supply. However, the sharp definition of the core region indicates that something other than osmotic pressure controls the desorption in this region and other explanations are considered here.

The unusual solvent behavior near the glassy core is a feature that is reported in work on solvent self-diffusion coefficients[12] and NMR relaxation times[12] in partially swollen PMMA rods. Both studies indicate that the polymer mobility decreases from the surface to the glassy core despite the solvent concentration being constant throughout the swollen regions. The smallest amplitude motions occur at the glassy core because the chains that exist in both the glass and the rubber are effectively fixed at the interface. The solvent self-diffusion and motions are impeded by the restricted motions of the polymer chains. The same restricted motions influence the core region in the $T_d$ image (Figure 5A). The polymer chains do not move easily in this region of the sample and are effectively trapping the solvent molecules.

The differences in $T_d$s are considerably smaller in the second stage with the minimum being 66 h at the surface and the maximum being 600 h around the glassy core. The changes in $T_d$s at the glassy core indicate that desorption has begun in that region. The increased $T_d$s in the bulk region indicate that desorption has slowed because the motions of the polymer and solvent are reduced sufficiently to restrict molecular transport out of the polymer. The surface region has smaller $T_d$s than in the first stage. The surface controls the desorption process and therefore should have a slower rates than the bulk region. The $T_d$s of the surface region are now smaller than those in the bulk which contradicts the rate-controlling idea. The reason for the smaller $T_d$s is that the surface region has lost sufficient solvent (and as a result has a significantly shorter $T_2$s) so that the signal drops into the noise level of the image. When the signal is below a threshold noise level, the $T_d$ calculation assigns those regions $T_d$s of zero. When the calculation includes some values above the threshold, calculated $T_d$s are much smaller than expected for the actual desorption rate at the surface.

In the third stage, the signal intensities (Figure 3H–K) are nearly uniform throughout the swollen region with a decrease near the surface. Likewise, the $T_d$s throughout the sample (Figure 5D,E) are uniform. During these time intervals, the entire swollen region is probably below $T_g$. Desorption is driven by osmotic pressure drawing the solvent toward the surface through the free volume in the polymer. However, desorption is restricted by the reduced polymer segmental mobility which is uniform throughout the swollen region. While further data are not available from this work, the $T_d$s are expected to remain uniform throughout the swollen polymer and to decrease with time.

## Conclusion

NMR imaging provides details of the desorption process not available by other techniques. These details indicate that the desorption processes in a partially swollen polymer are quite complex and extensive NMR imaging work is necessary to further understand the process. In this study, the overall controlling feature of desorption from any region is the solvent mobility regulated by the polymer segmental mobility. At the polymer surface, the polymer changes from a rubber to a glass because of the rapid solvent loss. The glassy surface reduces the overall desorption rate because of the limited polymer motions. At the glassy core, polymer chains associated with both the glass and the rubber have restricted motions severely limiting the solvent mobility and reducing the desorption rate from that region. Finally, once the polymer in the swollen region reaches a homogeneous motional state, the desorption continues at a constant rate throughout the sample.

**Acknowledgment.** We wish to thank the National Science Foundation for its support through the Materials Research Grant at Case Western Reserve University.

## References and Notes

(1) Gyor, M.; Rockenbauer, A.; Jokay, L.; Tudos, F. *Polym. Bull.* **1986**, *15*, 525.
(2) Thomas, N. L.; Windle, A. H. *Polymer* **1981**, *22*, 627.
(3) Hoh, K.-P.; Perry, B. C.; Rotter, G.; Ishida, H.; Koenig, J. L. *J. Adh.* **1989**, *27*, 245.
(4) Nieminen, A. O. K.; Koenig, J. L. *J. Adh. Sci. Tech.* **1989**, *2*, 407.
(5) Clough, R. C.; Koenig, J. L. *J. Polym. Sci., Polym. Lett. Ed.* **1989**, *27*, 451.
(6) Rothwell, W. P.; Gentempo, P. P. *Bruker Report* **1985**, *1*, 46.
(7) Rothwell, W. P.; Holecek, D. R.; Kershaw, J. A. *J. Polym. Sci., Polym. Lett. Ed.* **1984**, *22*, 241.
(8) Blackband, S.; Mansfield, P. *J. Phys. C: Solid State Phys.* **1986**, *19*, L49.
(9) Weisenberger, L. A.; Koenig, J. L. *J. Polym. Sci., Polym. Lett. Ed.* **1989**, *27*, 55.
(10) Weisenberger, L. A.; Koenig, J. L. *Polym. Prepr. (Am. Chem. Soc., Div. Polym. Chem.)* **1988**, *29*, 98.
(11) Weisenberger, L. A.; Koenig, J. L. *Appl. Spectrosc.* **1989**, Sept/Oct, *43*, No. 7.
(12) Weisenberger, L. A.; Koenig, J. L. *Macromolecules*, preceding paper in this issue.
(13) Andrew, E. R. *Acc. Chem. Res.* **1983**, *16*, 114.
(14) Budinger, T. F.; Lauterbur, P. C. *Science* **1984**, *226*, 288.
(15) Bailes, D. R.; Bryant, D. J. *Contemp. Phys.* **1984**, *24*, 441.
(16) Smith, S. L. *Anal. Chem.* **1985**, *57*, 595A.
(17) Pykett, I. L. *Sci. Am.* **1982**, *246*, 78.
(18) Luiten, A. L. *Essentials of Clinical MRI*; Falke, T. H. M., ed.; Martinus Nijhoff Publishers: Boston, 1988; p 3.
(19) Yamamoto, E.; Kohno, H. *IEEE Transactions on Medical Imaging* **1986**, *MI-5*, 229.
(20) Brown, T. R.; Kincaid, B. M.; Ugurbil, K. *Proc. Natl. Acad. Sci. U.S.A.* **1982**, *79*, 3523.
(21) Brateman, L. *Am. J. Rad.* **1986**, *146*, 971.
(22) Carr, H. Y.; Purcell, E. M. *Phys. Rev.* **1954**, *94*, 630.
(23) Meiboom, S.; Gill, D. *Rev. Sci. Instrum.* **1958**, *29*, 688.
(24) Thomas, N. L.; Windle, A. H. *Polymer* **1982**, *23*, 529.
(25) Hui, C.-Y.; Wu, K.-C.; Laskey, R. C.; Kramer, E. J. *J. Appl. Phys.* **1987**, *61*, 5137.
(26) Fox, T. G. *Bull. Am. Phys. Soc.* **1956**, 123.
(27) Downes, J. G.; McKay, B. H. *J. Polym. Sci.* **1959**, *36*, 130.
(28) Grayson, M. A.; Pao, P. S.; Wolf, C. J. *J. Polym. Sci., Polym. Phys. Ed.* **1987**, *25*, 935.